

Article

Design of a Fractional Order Frequency PID Controller for an Islanded Microgrid: A Multi-Objective Extremal Optimization Method

Huan Wang ^{1,2}, Guoqiang Zeng ^{2,*}, Yuxing Dai ^{1,2}, Daqiang Bi ³, Jingliao Sun ⁴ and Xiaoqing Xie ²

¹ College of Electrical and Information Engineering, Hunan University, Changsha 410082, China; wh83@wzu.edu.cn (H.W.); daiyx@hnu.edu.cn (Y.D.)

² National-Local Joint Engineering Laboratory of Digitalize Electrical Design Technology, Wenzhou University, Wenzhou 325035, China; xiaoqingxie@stu.wzu.edu.cn

³ State Key Laboratory of Power Systems and Department of Electrical Engineering, Tsinghua University, Beijing 100084, China; bidaqiang@tsinghua.edu.cn

⁴ State Grid Wenzhou Electric Power Supply Company, Wenzhou 325000, China; sunjingliao@163.com

* Correspondence: zeng.guoqiang5@gmail.com; Tel.: +86-159-6740-5738

Received: 23 August 2017; Accepted: 22 September 2017; Published: 1 October 2017

Abstract: Fractional order proportional-integral-derivative(FOPID) controllers have attracted increasing attentions recently due to their better control performance than the traditional integer-order proportional-integral-derivative (PID) controllers. However, there are only few studies concerning the fractional order control of microgrids based on evolutionary algorithms. From the perspective of multi-objective optimization, this paper presents an effective FOPID based frequency controller design method called MOEO-FOPID for an islanded microgrid by using a Multi-objective extremal optimization (MOEO) algorithm to minimize frequency deviation and controller output signal simultaneously in order to improve finally the efficient operation of distributed generations and energy storage devices. Its superiority to nondominated sorting genetic algorithm-II (NSGA-II) based FOPID/PID controllers and other recently reported single-objective evolutionary algorithms such as Kriging-based surrogate modeling and real-coded population extremal optimization-based FOPID controllers is demonstrated by the simulation studies on a typical islanded microgrid in terms of the control performance including frequency deviation, deficit grid power, controller output signal and robustness.

Keywords: microgrid; fractional order controller; frequency control; multi-objective optimization; extremal optimization

1. Introduction

Microgrids have been widely considered as a building block of future smart grid [1], so there have been many real islanded microgrid systems developed for rural and distant areas [2–5]. However, how to control the voltage and frequency of a microgrid in an islanded model has been one of the major challenges for researchers recently [6], because it is often more difficult than—in grid-connected mode. More specifically, when the microgrids operate in the grid-connected mode, the control of voltage and frequency depends on the regulation of the main utility grid. While the microgrids are in the islanded mode, the distributed components should regulate the stochastic and determinate fluctuation caused by some distributed generations, e.g., wind turbine generator and solar photovoltaics, and demand-side loads.

In recent years, some frequency control methods for microgrids or hybrid power systems have been proposed by using traditional proportional-integral-derivative (PID) controllers or robust

controllers [7–16]. For example, a hybrid method by combining particle swarm optimization (PSO) and fuzzy logic [11] is proposed to design proportional-integral (PI)-based frequency controllers for an alternating current microgrid. Another genetic algorithm (GA)-based frequency PID controller has been developed for a solar thermal diesel wind hybrid energy generation and storage system [13]. Singh et al. [14] present a robust PSO-based H_∞ method for the frequency control of a hybrid power system. Similar research works include robust H_∞ and structured singular value μ -based control synthesis approaches for microgrids [15]. Bendato et al. [16] proposed an effective two-step procedure to optimize a real-time energy management system by integrating economic aspects and power quality objectives including reactive power, voltage and frequency. Its effectiveness has been demonstrated on a microgrid system called “University of Genoa Smart Polygeneration Microgrid”.

Fractional order controllers have attracted increasing attentions recently due to their better control performance compared to traditional integer-order controllers [17–24]. Consequently, there are some recently reported frequency control methods based on fractional order proportional-integral-derivative (FOPID) controllers for islanded microgrids by using some intelligent optimization algorithms, e.g., Kriging-based surrogate modeling, called the KSM method [25], chaotic PSO based fractional order fuzzy PID controller [26]. In addition, Pan and Das [27] utilized a chaotic nondominated sorting genetic algorithm-II (NSGA-II) algorithm to design fractional order PID controllers for load-frequency control of two interconnected power systems by considering the two conflicting time domain objectives, including the integral of time multiplied squared error of frequency deviation, and the integral of the squared deviation in the controller output. These research results have also shown that the proposed chaotic NSGA-II-based FOPID controller performs better than the standard PID controller under nominal operating and perturbed operating conditions. On the other hand, these research works have also indicated that the optimization algorithms play critical roles in the performance of FOPID controllers. Consequently, how to design intelligent optimization methods especially multi-objective evolutionary algorithms to further improve the comprehensive performance of FOPID controllers for frequency control of islanded microgrids is of great practical significance.

Extremal optimization (EO) [28,29] is a novel evolutionary optimization framework differing from traditional optimization algorithms due to its prominent far-from-equilibrium characteristics, imitating the theory of self-organized criticality [30]. In contrast to favoring the good in traditional evolutionary algorithms, EO always selects the bad elements or individuals for mutation based on a whole random or power-law probability distribution. Consequently, EO has attracted increasing attention recently for its wide applications in various benchmark and real-world engineering optimization problems [31,32]. However, there are only few multi-objective evolutionary algorithms based on the EO mechanism [33–37]. An individual elitist $(1+\lambda)$ multi-objective extremal optimization algorithm [33] is based on a single solution and a hybrid mutation operator combining Gaussian mutation with Cauchy mutation to enhance the exploratory capabilities. In our recent research work, a modified multi-objective extremal optimization based on individual iterated optimization mechanisms has been presented to design FOPID controllers for automatic voltage regulator systems [37]. On the other hand, another version called multi-objective population-based extremal optimization (MOPEO) is proposed by combining population-based optimization mechanism and a popular mutation operator called non-uniform mutation [34]. Furthermore, an improved version is proposed by adopting population-based iterated optimization, a more effective mutation operation called polynomial mutation, and a novel and more effective mechanism for generating new population [36].

Unfortunately, to the best of our knowledge, there are few reported research works concerning the application of EO into the control of microgrids and other power systems, let alone multi-objective EO algorithms into microgrids. This paper proposes a multi-objective extremal optimization (MOEO)-based FOPID method called MOEO-FOPID for the fractional order frequency control of an islanded microgrid in order to improve the efficient operation of distributed generations and energy storage devices. Its superiority to other recently reported single-objective evolutionary

algorithms-based FOPID [22,25], and NSGA-II-based FOPID/PID controllers [20,38] will be demonstrated by the simulation results for the typical case of an islanded microgrid.

The rest of this paper is structured as follows. Some basic definitions of a FOPID controller and multi-objective optimization are introduced briefly in Section 2. Section 3 presents a small-signal model of an islanded microgrid. Then, a MOEO-FOPID method for the frequency control of an islanded microgrid is proposed in Section 4. Section 5 gives the simulation results for a typical microgrid to demonstrate the superiority of MOEO-FOPID to other reported optimization algorithms-based FOPID and PID controllers. Finally, some concluding remarks are presented in Section 6.

2. Preliminaries

2.1. FOPID Controller

As one of three widely used definitions for fractional differentiation and integration, the Riemann Liouville (RL) definition is presented as follows [19]:

$${}_a D_t^r f(t) = \frac{1}{\Gamma(n-r)} \frac{d^n}{dt^n} \int_a^t \frac{f(\tau)}{(t-\tau)^{r-n+1}} d\tau, \quad n-1 < r < n \quad (1)$$

where $\Gamma(\cdot)$ is the Gamma function. The Laplace transform of Equation (1) is defined as the following form:

$$\int_0^\infty e^{-st} {}_a D_t^r f(t) dt = s^r F(s) - \sum_{k=0}^{n-1} s^k {}_0 D_t^r f(t)|_{t=0} \quad (2)$$

Figure 1 shows a block diagram of a closed-loop control system with a FOPID controller called a $PI^\lambda D^\mu$ controller [17]. Its transfer function model is defined as follows:

Definition 1. The transfer function $G_c(s)$ of a FOPID controller is described as follows:

$$G_c(s) = \frac{U(s)}{E(s)} = K_p + K_i s^{-\lambda} + K_d s^\mu \quad (3)$$

where $U(s)$ and $E(s)$ are the transfer functions of control signal and error signal, respectively; and K_p , K_i and K_d are the gains of proportional, integral, and derivative, respectively. λ and μ are the order numbers of the fractional order integrator and differentiator, respectively. Generally, the domain of λ and μ are defined as: $0 \leq \lambda \leq 2$ and $0 \leq \mu \leq 2$. It is clear that the traditional PID controller is one special case of a FOPID controller when $\lambda = 1$ and $\mu = 1$.

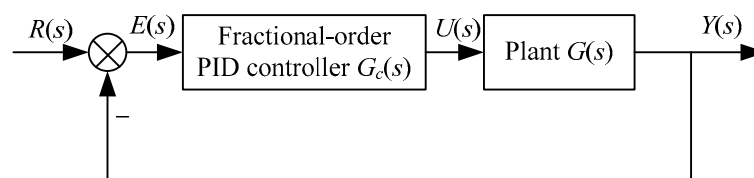


Figure 1. Block diagram of a closed-loop control system with a FOPID controller.

The control signal $u(t)$ from the output of the $PI^\lambda D^\mu$ controller is computed as the following Equation:

$$u(t) = K_p e(t) + K_i D^{-\lambda} e(t) + K_d D^\mu e(t) \quad (4)$$

where $e(t)$ is the error signal.

2.2. Multi-Objective Optimization

Formally, a multi-objective unconstrained minimization problem is defined as the following Equation [39]:

$$\begin{aligned} &\text{minimize } F(\mathbf{x}) = (f_1(\mathbf{x}), f_2(\mathbf{x}), \dots, f_m(\mathbf{x})) \\ &\text{s.t. } \mathbf{L} \leq \mathbf{x} \leq \mathbf{U} \end{aligned} \tag{5}$$

where $\mathbf{x} = (x_1, x_2, \dots, x_n) \in \Omega$ is a decision vector consisting of n decision variables x_1, x_2, \dots, x_n , $\Omega \subseteq \mathbb{R}^n$ is the decision space, m is the number of objective functions, \mathbf{L} and \mathbf{U} represent the lower and upper bounds of vector \mathbf{x} , respectively, $F: \Omega \rightarrow \mathbb{R}^m$ consists of m real-valued objective functions and \mathbb{R}^m is defined as the m dimensions objective space.

An objective vector $\mathbf{u} = (u_1, u_2, \dots, u_m) \in \mathbb{R}^m$ is considered to dominate another objective vector $\mathbf{v} = (v_1, v_2, \dots, v_m) \in \mathbb{R}^m$, which is denoted as $\mathbf{u} \prec \mathbf{v}$ if and only if the following two conditions are satisfied simultaneously: (1) $\forall i \in \{1, 2, \dots, m\}, u_i \leq v_i$, and (2) $\exists i \in \{1, 2, \dots, m\}, u_i < v_i$. A decision vector $\mathbf{x} \in \Omega$ is defined to be non-dominated or Pareto optimal if and only if there does not exist another decision vector $\mathbf{x}^* \in \Omega$ such that $F(\mathbf{x}^*) \prec F(\mathbf{x})$. The Pareto-optimal set is defined as all Pareto optimal solutions in Ω . The set of m objective functions values corresponding to the Pareto-optimal set are called Pareto front.

3. Microgrid Models Based on Small-Signal Analysis

There are some reported research works concerning small-signal analysis for hybrid distributed generation systems or microgrids [8–10]. Figure 2 presents a block diagram of a typical islanded microgrid [25]. The transfer functions and model parameters of distributed energy power generations including wind turbine generator (WTG), solar photovoltaic (PV) system, diesel engine generator (DEG), fuel cell (FC), and energy storage systems, e.g., battery energy storage system (BESS) and flywheel energy storage system (FESS) are described as Table 1. Here, Δf is the frequency deviation; u is the control signal from FOPID based frequency controller; P_{sol} and P_W are the input stochastic power of PV and WTG, respectively; $P_{PV}, P_{WTG}, P_{DEG}, P_{FC}, P_{BESS}$ and P_{FESS} are the output power of PV, WTG, DEG, FC, BESS and FESS, respectively, and P_L is the variable load power. Some intermediate variables are computed as follows: $P_t = P_{PV} + P_{WTG}$, $P_S = P_t + P_{FC} + P_{DEG} - P_{BESS} - P_{FESS}$, and $P_e = P_L - P_S$.

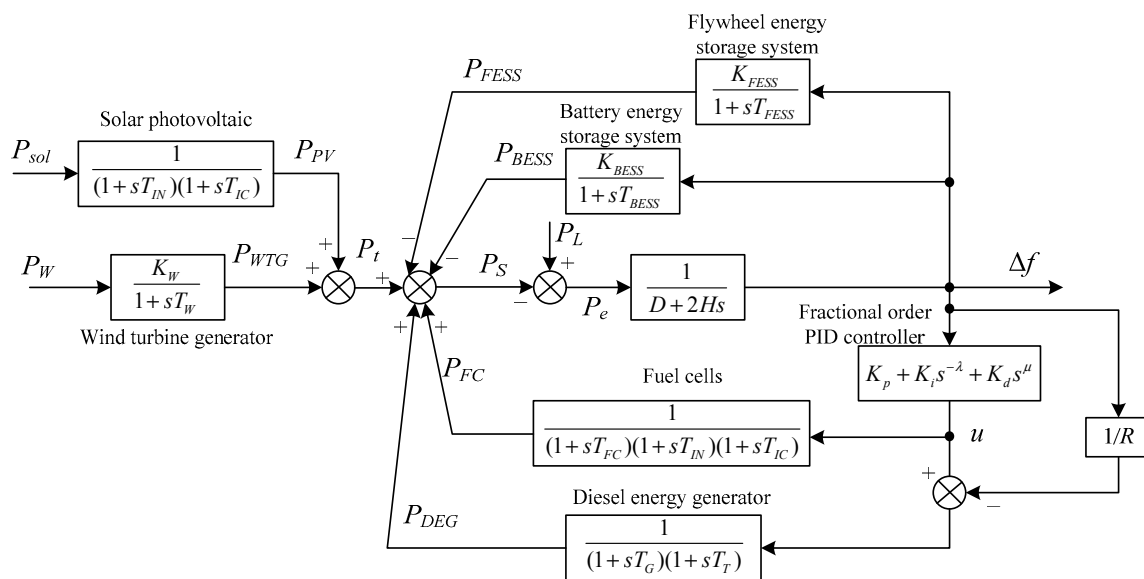


Figure 2. Block diagram of an islanded microgrid with small-signal models.

We consider large deterministic drift and random fluctuations for solar photovoltaic generation, wind generation, and demand-side loads, which are described as the following general model [13]:

$$P = \frac{(\phi\eta\sqrt{\beta}(1 - G(s)) + \beta)\Gamma}{\beta} = \chi\Gamma \tag{6}$$

where P is the stochastic power, ϕ represents the stochastic component and β is a parameter that contributes to the mean value of the power, respectively. $G(s)$ denotes the transfer function of a low pass filter; η is a normalized parameter to make the generated or demand power χ match the per unit (pu) level; and Γ describes a time-variable signal of fluctuation for stochastic power output. The detailed parameters of stochastic models for distributed generators and demand load are given as Table 2. Here, $U(-1, 1)$ presents random uniform function between -1 and 1 , and $H(t)$ denotes Heaviside step function. Figure 3 illustrates the realization of the stochastic powers of WTG, PV and demand-side loads.

Table 1. The small-signal analysis models and parameters of the components of an islanded microgrid [25].

Component	Transfer Function	Parameters
Wind turbine generator (WTG)	$G_{WTG}(s) = \frac{\Delta P_{WTG}}{\Delta P_W} = \frac{K_W}{1+sT_W}$	$K_W = 1, T_W = 1.5$ s
Solar photovoltaic (PV)	$G_{STPG}(s) = \frac{\Delta P_{PV}}{\Delta P_{sol}} = \frac{1}{(1+sT_{IN})(1+sT_{IC})}$	$T_{IN} = 0.04$ s, $T_{IC} = 0.004$ s
Fuel cell (FC)	$G_{FC}(s) = \frac{\Delta P_{FC}}{\Delta u} = \frac{1}{(1+sT_{FC})(1+sT_{IN})(1+sT_{IC})}$	$K_{FC} = 1, T_{FC} = 0.26$ s
Diesel energy generator (DEG)	$G_{DEG}(s) = \frac{\Delta P_{DEG}}{\Delta u} = \frac{1}{(1+sT_G)(1+sT_T)}$	$T_G = 0.08$ s, $T_T = 0.4$ s
Microgrid system	$G_S(s) = \frac{\Delta f}{\Delta P_e} = \frac{1}{D+2Hs}$	$D = 0.015$ pu/Hz, $H = 1/12$ pu.sec, $R = 3$ Hz/pu
Flywheel energy storage system (FESS)	$G_{FESS}(s) = \frac{\Delta P_{FESS}}{\Delta f} = \frac{K_{FESS}}{1+sT_{FESS}}$	$K_{FESS} = 1, T_{FESS} = 0.1$ s
Battery energy storage system (BESS)	$G_{BESS}(s) = \frac{\Delta P_{BESS}}{\Delta f} = \frac{K_{BESS}}{1+sT_{BESS}}$	$K_{BESS} = 1, T_{BESS} = 0.1$ s

Table 2. The parameters of stochastic models for distributed generators and demand load.

Stochastic Models	Model Parameters
Wind power generation	$\phi \sim U(-1, 1), \eta = 0.8, \beta = 10, G(s) = 1/(10^4s + 1), \Gamma = 0.24H(t) - 0.04H(t - 140)$
Solar power generation	$\phi \sim U(-1, 1), \eta = 0.1, \beta = 10, \delta = 0.1, G(s) = 1/(10^4s + 1), \Gamma = 0.05H(t) + 0.02H(t - 180)$
Demand loads	$\phi \sim U(-1, 1), \eta = 0.9, \beta = 10, G(s) = (300/(300s + 1)) + (1/(1800s + 1)), \Gamma = (1/\chi)[0.9H(t) + 0.03H(t - 110) + 0.03H(t - 130) + 0.03H(t - 150) - 0.15H(t - 170) + 0.1H(t - 190)] + 0.02H(t)$

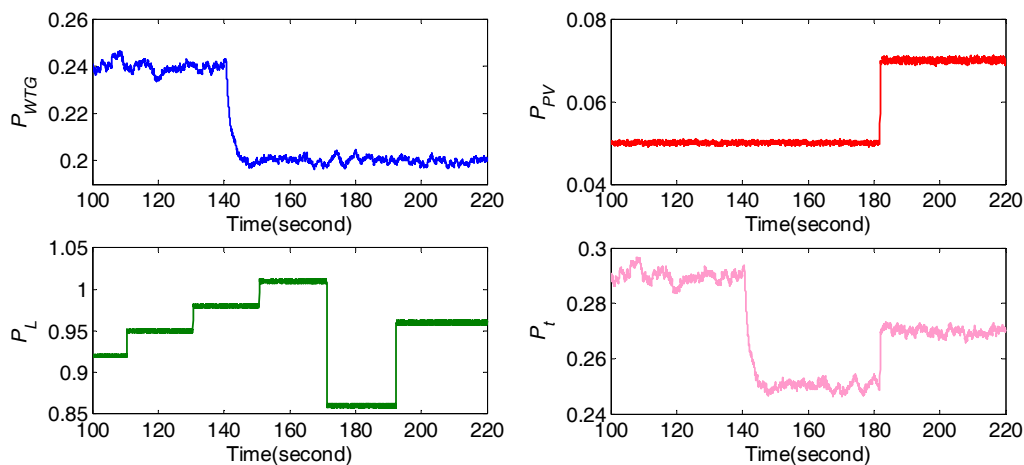


Figure 3. Stochastic powers of WTG (labeled P_{WTG}), PV (labeled P_{PV}), demand-side loads (labeled P_L), and the sum of WTG and PV generation (labeled P_t).

4. Multi-Objective Extremal Optimization Based FOPID Method for the Frequency Control of Islanded Microgrids

In order to obtain good frequency control performance for an islanded microgrid, both the frequency deviation (Δf) in the microgrid and the control output signal (u) of the FOPID controller are expected to be minimized, yet these two objectives are generally conflictive. Consequently, the frequency control problem of an islanded microgrid based on a FOPID controller is formulated to a typical multi-objective optimization problem. The detailed formulation is as follows.

Definition 2. The following two objectives F_1 and F_2 subject to some given constraints are defined to evaluate the performance of a FOPID controller $\mathbf{x} = (K_p, K_i, K_d, \lambda, \mu)$ for the frequency control of an islanded microgrid.

$$\min\{F_1(\mathbf{x}), \min\{F_2(\mathbf{x})\}, \mathbf{x} = (K_p, K_i, K_d, \lambda, \mu) \tag{7}$$

$$F_1(\mathbf{x}) = \int_{T_{\min}}^{T_{\max}} (\Delta f)^2 dt \tag{8}$$

$$F_2(\mathbf{x}) = \int_{T_{\min}}^{T_{\max}} u^2 dt \tag{9}$$

$$s.t. \begin{cases} |P_{FESS}| < P_{FESSmax}, & |P_{BESS}| < P_{BESSmax}, \\ 0 < P_{FC} < P_{FCmax}, & 0 < P_{DEG} < P_{DEGmax}, \\ |P_{FESSr}| < P_{FESSrmax}, & |P_{BESSr}| < P_{BESSrmax}, \\ |P_{FCr}| < P_{FCrmax}, & |P_{DEGr}| < P_{DEGrmax}, \\ \mathbf{L} \leq \mathbf{x} \leq \mathbf{U} \end{cases} \tag{10}$$

where $P_{FESSmax}, P_{BESSmax}, P_{FCmax}, P_{DEGmax}$ are the output saturations (in pu) of $P_{FESS}, P_{BESS}, P_{FC}, P_{DEG}$, respectively; $P_{FESSr}, P_{BESSr}, P_{FCr}, P_{DEGr}$ are the rate of $P_{FESS}, P_{BESS}, P_{FC}, P_{DEG}$, respectively; $P_{FESSrmax}, P_{BESSrmax}, P_{FCrmax}, P_{DEGrmax}$ are the maximum constraints of $P_{FESSr}, P_{BESSr}, P_{FCr}, P_{DEGr}$, respectively; and \mathbf{L} and \mathbf{U} represent the lower and upper bounds of the FOPID controller parameters, respectively.

In this paper, a multi-objective extremal optimization based FOPID method, called MOEO-FOPID, is proposed to solve the aforementioned multi-objective optimization problem. Figure 4 presents the flowchart of the proposed MOEO-FOPID-based frequency controller optimal design algorithm for an islanded microgrid.

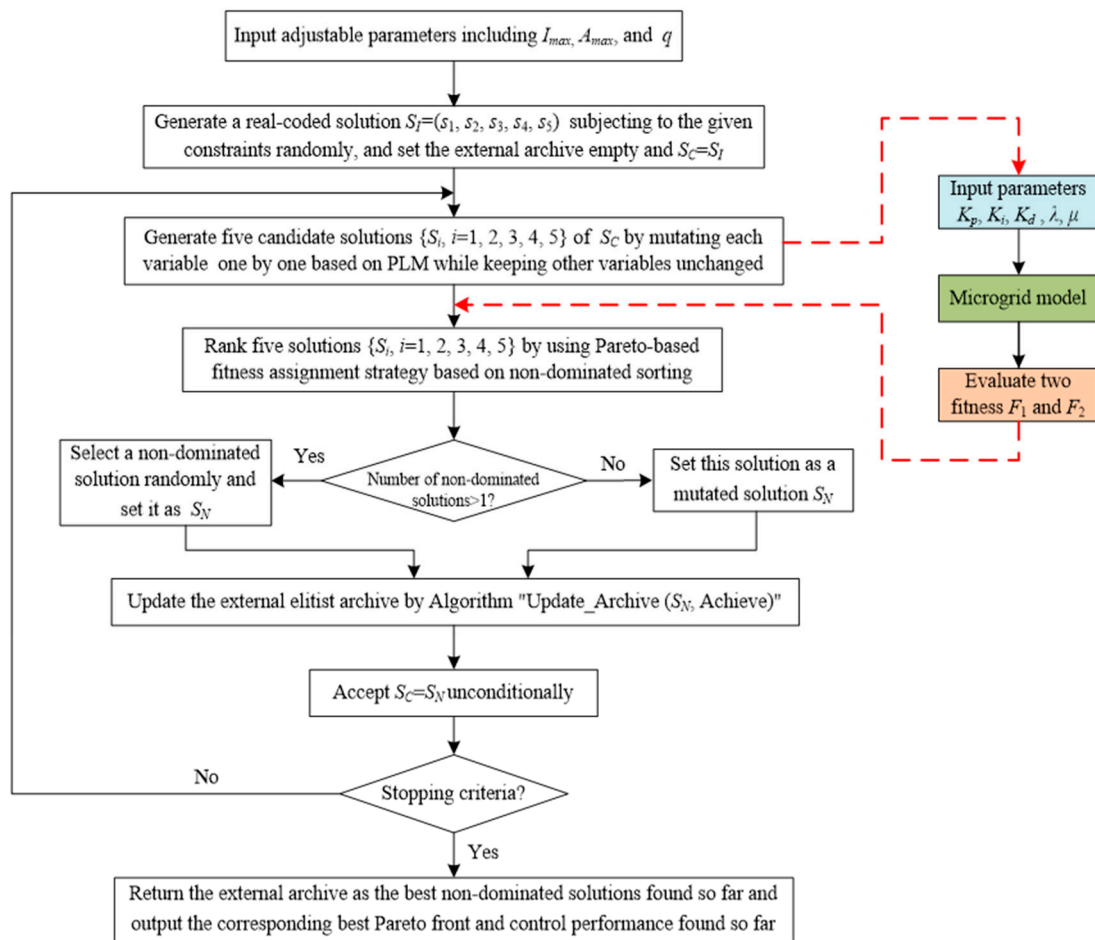


Figure 4. Flowchart of the proposed MOEO-FOPID method for the frequency control of microgrids.

MOEO-FOPID-Based Frequency Controller Optimal Design Algorithm for an Islanded Microgrid

Input: A microgrid system with a FOPID-based frequency controller and adjustable parameters used in the MOEO-FOPID algorithm, including the maximum number of iterations I_{max} , the maximum size of external archive A_{max} , and the shape parameter q used in mutation operation.

Output: The best non-dominated solutions for the designed FOPID-based frequency controller and the corresponding best Pareto front found so far.

Step 1: Generate a real-coded solution $S = (s_1, s_2, s_3, s_4, s_5)$ representing the control parameters of a FOPID-based frequency controller $(K_p, K_i, K_d, \lambda, \mu)$ in an islanded microgrid subject to the given constraints (10) randomly, and set the external archive A as empty and $S_C = S$.

Step 2: By mutating each variable s_i ($i = 1, 2, 3, 4, 5$) of the current solution S_C one-by-one based on multi-non-uniform mutation (MNUM) while keeping other variables unchanged, generate five candidate solutions $\{S_i, i = 1, 2, 3, 4, 5\}$. The detailed process is formulated as follows:

$$S_i = \begin{cases} S_C + (\mathbf{U} - S_C) \times A(t), & \text{if } r < 0.5, \\ S_C + (S_C - \mathbf{L}) \times A(t), & \text{if } r \geq 0.5. \end{cases} \quad (11)$$

$$A(t) = \left[r_1 \left(1 - \frac{I_C}{I_{max}} \right) \right]^q \quad (12)$$

where I_C is the number of current iterations in the optimization process, both r and r_1 are uniform random numbers between 0 and 1, and q is the shape parameter used in MNUM.

- Step 3:** Rank five solutions $\{S_i, i = 1, 2, 3, 4, 5\}$ based on the non-dominated sorting strategy, where the two objective functions F_1 and F_2 are evaluated by Definition 2.
- Step 4:** If the number of non-dominated solutions is just one, then select the only non-dominated solution S_{nd} as the new solution S_N ; otherwise, select one from several non-dominated solutions randomly, and set this one as the new solution S_N .
- Step 5:** Update **A** by algorithm “Update_Archive (S_N , Achieve)” [37] shown in Algorithm 1.
- Step 6:** Accept $S_C = S_N$ unconditionally.
- Step 7:** If the predefined stopping criteria, e.g., maximum number of iterations I_{max} is met, then return to Step 2; otherwise, go to Step 8.
- Step 8:** Return external archive **A** as the best non-dominated solutions for the FOPID controller for the frequency control of an islanded microgrid, and output the best Pareto front found so far and the corresponding control performance.

Algorithm 1 The Pseudo-Code of Algorithm “Update_Archive (S_N , Archive)” [37]

```

1: Begin
2: If the solution  $S_N$  is dominated by at least one member of the archive, then
3: The archive keeps unchanged
4: Else if some members of archive are dominated by  $S_N$ , then
5: Remove all the dominated members from the archive and add  $S_N$  to the archive
6: End if
7: Else
8: If the number of archive is smaller than  $A_{max}$ , i.e., the predefined maximum number of the archive, then
9: Add  $S_N$  to the archive
10: Else
11: If  $S_N$  resides in the most crowded region of the archive, then
12: The archive keeps unchanged
13: Else
14: Replace the member in the most crowded region of the archive by  $S_N$ 
15: End if
16: End if
17: End if
18: End

```

5. Simulation Results

5.1. Performance Comparison in Nominal Microgrid Conditions

This section presents the simulation results for an islanded microgrid in order to demonstrate the superiority of the proposed MOEO-FOPID method to the NSGA-II-based FOPID/PID [20,38] and the reported single-objective-optimization-algorithms-based FOPID method [22,25,40]. The parameters of the output saturations and rate constraints for the different elements in this microgrid are set as $P_{FESSmax} = P_{BESSmax} = 0.11$, $P_{FCmax} = 0.48$, $P_{DEGmax} = 0.45$, $P_{FESSrmax} = P_{BESSrmax} = 0.05$, $P_{FCrmax} = 1$, and $P_{DEGrmax} = 0.5$. For the sake of fair comparison, the lower and upper bounds of the FOPID controller parameters are set the same as in [25]: $\mathbf{L} = [0, 0, 0, 0, 0]$ and $\mathbf{U} = [5, 5, 5, 2, 2]$. The parameters for MOEO and NSGA-II used in the experiments are shown in Table 3. Note that there are three main differences between MOEO-FOPID and NSGA-II-FOPID. Firstly, MOEO-FOPID adopts an individual-based iterated optimization mechanism, while NSGA-II-FOPID uses a population based optimization mechanism. Secondly, MOEO-FOPID has only selection and mutation operations while NSGA-II-FOPID has more operations including selection, crossover and mutation. Thirdly, MOEO-FOPID has fewer adjustable parameters than NSGA-II-FOPID. As a

consequence, MOEO-FOPID is considered to be simpler than NSGA-II-FOPID from the perspective of algorithm design.

Table 3. The parameters for MOEO-FOPD/PID and NSGA-II-FOPID/PID used in the experiments.

Algorithm	Parameters
NSGA-II-FOPID/PID [20,38]	$I_{\max} = 500$, population size $NP = 30$, crossover probability $p_c = 0.9$, mutation probability $p_m = 1/n$, distribution indexes $\eta_c = 20$ and $\eta_m = 20$ for simulated binary crossover (SBX) and PLM
MOEO-FOPID/PID	$I_{\max} = 500$, $A_{\max} = 30$, $q = 6$

The statistical performance metrics of each algorithm were obtained by 30 independent runs. Table 4 shows the statistical results for the Pareto fronts obtained by MOEO and NSGA-II for the microgrid. More specifically, these metrics include the minimum, median, maximum, mean values and standard deviation of the hypervolume indicator (HI), spacing metric (SP), inertia-based diversity metric (I), and inverted generational distance (IGD), which are defined in [27,39]. It is obvious that MOEO-FOPID performed best in terms of the minimum, median, maximum, mean values of all the four metrics.

Table 4. Comparison of the statistical performance metric for Pareto fronts obtained by MOEO-FOPD/PID and NSGA-II-FOPID/PID for microgrid.

Performance Metrics	Algorithm	Minimum	Median	Maximum	Mean	Standard Deviation
Hypervolume indicator (HI, min)	NSGA-II-PID	1.83×10^{-4}	2.07×10^{-4}	2.26×10^{-4}	2.06×10^{-4}	1.15×10^{-5}
	MOEO-PID	1.26×10^{-4}	2.16×10^{-4}	3.92×10^{-4}	2.24×10^{-4}	7.78×10^{-5}
	NSGA-II-FOPID	1.56×10^{-4}	2.03×10^{-4}	3.35×10^{-4}	2.13×10^{-4}	5.08×10^{-5}
	MOEO-FOPID	1.04×10^{-4}	1.63×10^{-4}	2.20×10^{-4}	1.63×10^{-4}	2.95×10^{-5}
Spacing metric (SP, max)	NSGA-II-PID	5.41×10^{-3}	9.93×10^{-3}	1.50×10^{-2}	1.00×10^{-2}	2.69×10^{-3}
	MOEO-PID	4.28×10^{-3}	1.20×10^{-2}	2.32×10^{-2}	1.26×10^{-2}	5.43×10^{-3}
	NSGA-II-FOPID	6.93×10^{-3}	1.59×10^{-2}	2.84×10^{-2}	1.52×10^{-2}	4.56×10^{-3}
	MOEO-FOPID	1.91×10^{-3}	4.24×10^{-3}	7.97×10^{-3}	4.61×10^{-3}	1.22×10^{-3}
Inertia-based diversity metric (I, max)	NSGA-II-PID	7.07×10^{-2}	0.107	0.120	0.103	1.30×10^{-2}
	MOEO-PID	6.50×10^{-2}	6.15×10^{-2}	4.35×10^{-2}	6.01×10^{-2}	4.28×10^{-3}
	NSGA-II-FOPID	0.131	0.103	5.78×10^{-2}	0.103	2.14×10^{-2}
	MOEO-FOPID	0.135	0.117	8.10×10^{-2}	0.113	1.69×10^{-2}
Inverted generational distance (IGD, min)	NSGA-II-PID	7.00×10^{-3}	8.08×10^{-3}	9.58×10^{-3}	8.09×10^{-3}	6.16×10^{-4}
	MOEO-PID	9.52×10^{-3}	1.07×10^{-2}	1.38×10^{-2}	1.08×10^{-2}	9.43×10^{-4}
	NSGA-II-FOPID	3.43×10^{-3}	5.52×10^{-3}	9.22×10^{-3}	5.66×10^{-3}	1.17×10^{-3}
	MOEO-FOPID	3.16×10^{-3}	4.39×10^{-3}	1.20×10^{-2}	4.68×10^{-3}	1.59×10^{-3}

The best Pareto fronts for the FOPID/PID controllers, corresponding to the best HI values obtained by NSGA-II and MOEO, are compared in Figure 5. Clearly, the Pareto front obtained by MOEO-FOPID is closer to the “real” Pareto front. Furthermore, Table 5 shows the best FOPID/PID controller parameters and the best fitness values corresponding to the best HI performance obtained by MOEO and NSGA-II. It is evident that MOEO-FOPID has the best fitness values of F_1 and F_2 .

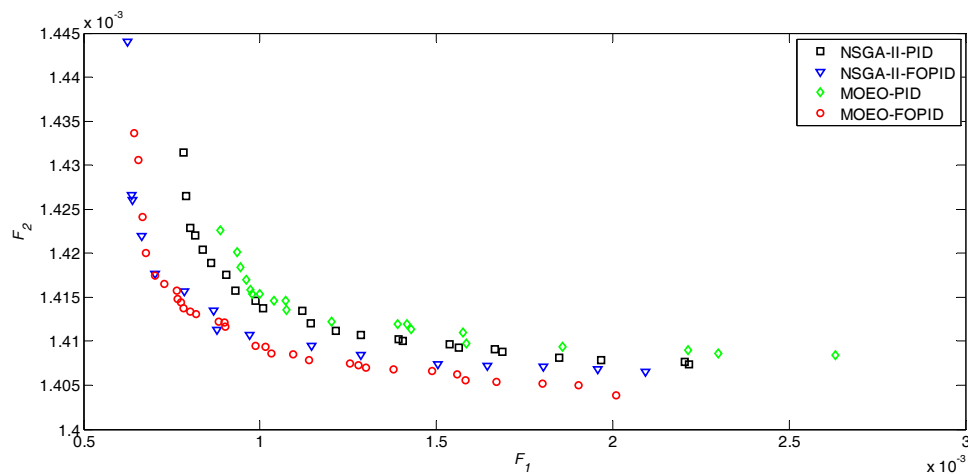
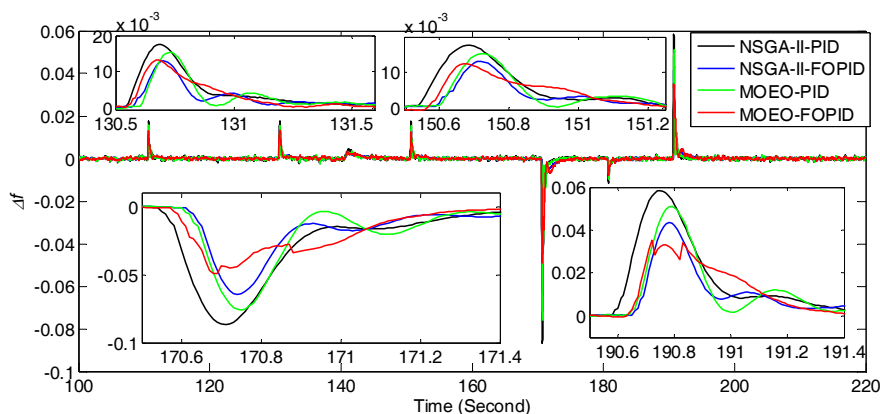


Figure 5. Comparison of Pareto fronts for PID/FOPID controllers obtained by NSGA-II and MOEO for the microgrid under the minimum values of HI.

Table 5. Best FOPID/PID controller parameters and performance obtained by MOEO and NSGA-II under the minimum values of HI.

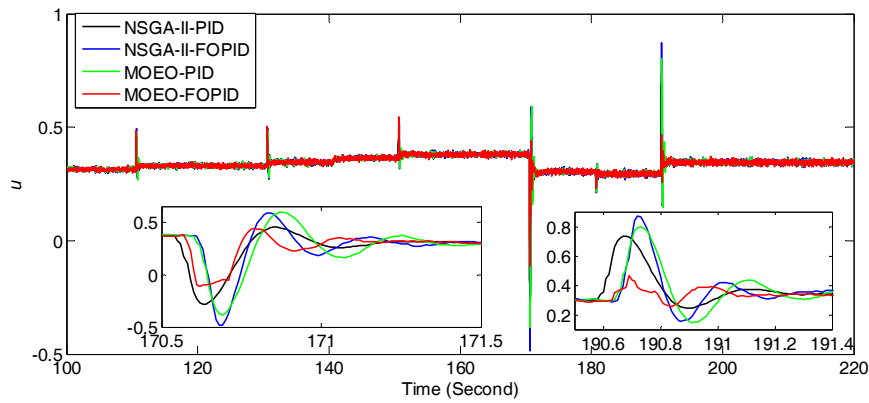
Algorithm	F_1	F_2	K_p	K_i	K_d	λ	μ
NSGA-II-PID	8.3877×10^{-4}	1.4204×10^{-3}	4.78192	4.76904	0.95045	1	1
MOEO-PID	8.1589×10^{-4}	1.4250×10^{-3}	4.53357	4.85426	1.05329	1	1
NSGA-II-FOPID	7.8307×10^{-4}	1.4198×10^{-3}	5	4.99475	0.54391	1.00950	1.20039
MOEO-FOPID	7.2219×10^{-4}	1.4174×10^{-3}	4.90695	4.16141	0.78012	1.00730	1.13911

Figure 6 compares the frequency deviation (Δf), control signal (u) and deficit power deviation (ΔP) of the microgrid with the best FOPID/PID controllers obtained by NSGA-II and MOEO. Clearly, MOEO-FOPID performed better than NSGA-II-FOPID/PID and MOEO-PID due not only to its smaller frequency fluctuation, grid power deficit and control signal, but also to its faster transient response. Similarly, the individual powers of the different components of the microgrid with the best FOPID/PID controllers obtained by NSGA-II and MOEO are compared in Figure 7. It is clear that the individual power fluctuations obtained by MOEO-FOPID are also the smallest.

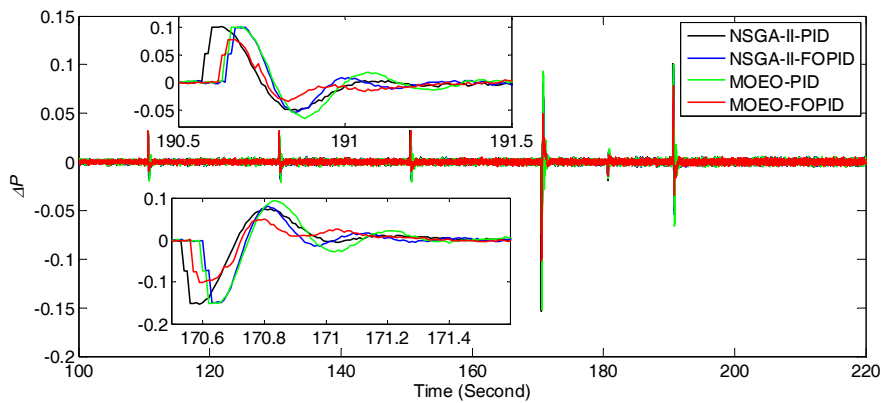


(a) Frequency deviation Δf

Figure 6. Cont.

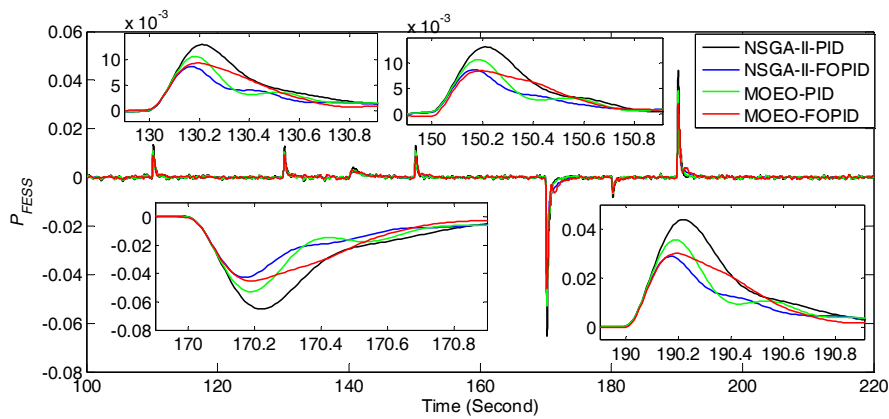


(b) Control signal u



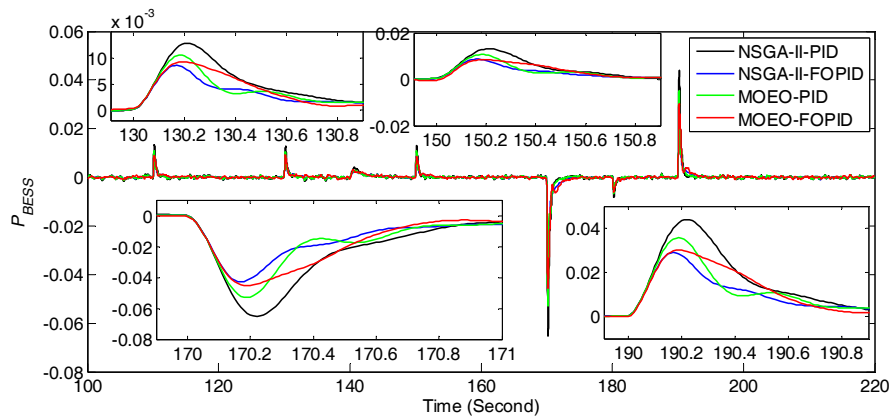
(c) Deficit power deviation ΔP

Figure 6. Comparison of frequency deviation Δf (a), control signal u (b) and deficit power deviation ΔP (c) of the test microgrid with the best FOPID/PID controllers obtained by the NSGA-II and MOEO algorithms.

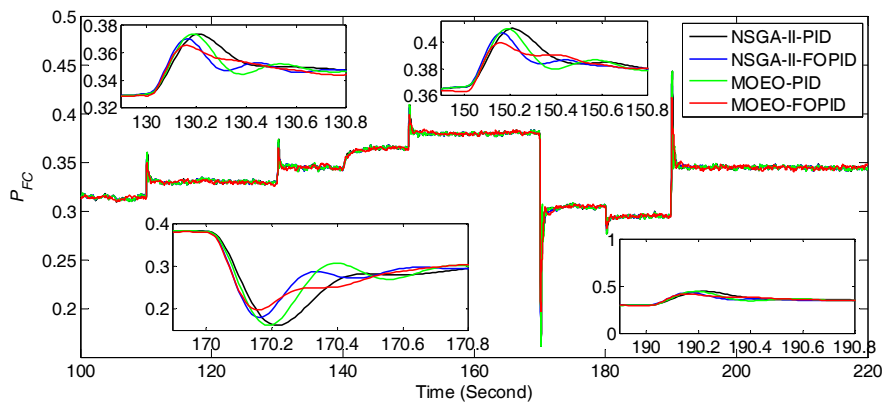


(a) Power of FESS labeled as P_{FESS}

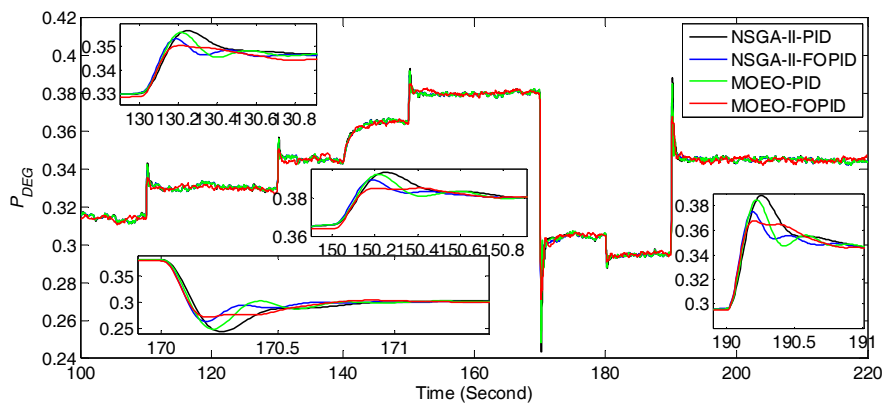
Figure 7. Cont.



(b) Power of BESS labeled as P_{BESS}



(c) Power of FC labeled as P_{FC}



(d) Power of DEG labeled as P_{DEG}

Figure 7. Comparison of individual powers in the different components of the test microgrid with the best FOPID/PID controllers obtained by the NSGA-II and MOEO algorithms.

It should be noted that the FOPID based on Kriging-based surrogate modeling, called KSM-FOPID, with a spline correlation model has been demonstrated to be superior to KSM-FOPID with other correlation models, GA-FOPID and GA-PID [25]. In order to further demonstrate the effectiveness of MOEO-FOPID, Table 6 presents the comparative results of MOEO-FOPID with recently reported single-objective evolutionary algorithms, e.g., KSM-FOPID [25] and real-coded population-EO-based FOPID called RPEO-FOPID [22]. In this experiment, the population size and maximum generations used in RPEO-FOPID are the same as KSM-FOPID, which are set as 10 and 15, respectively, and the

mutation parameter used in RPEO-FOPID is set as two. In the sake of fair comparison, the performance metric J was adopted as the same as that defined in [25].

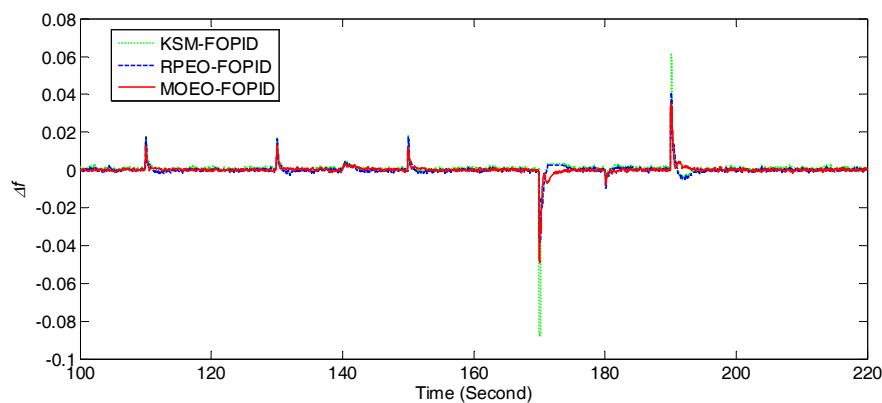
$$J = \int_{T_{\min}=100}^{T_{\max}=220} [w(\Delta f)^2 + ((1-w)/K_n)u^2] dt \quad (13)$$

where the weighted parameter w is set as 0.7, and the normalizing constant K_n is set as 10^4 .

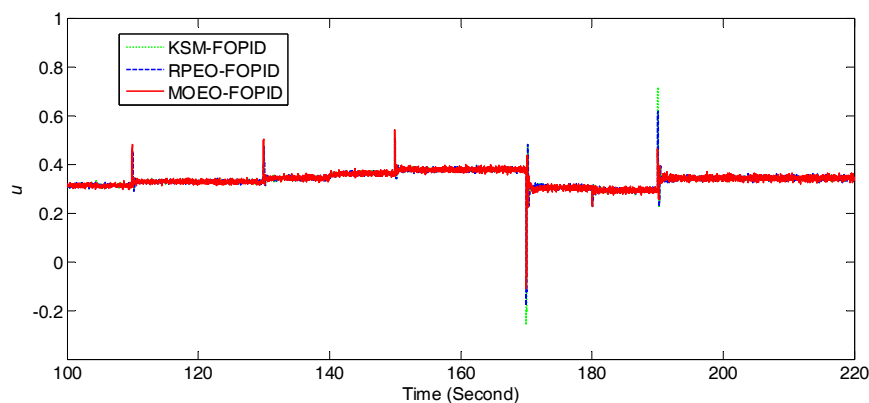
Table 6. Best FOPID controller parameters and performance obtained by MOEO-FOPID, RPEO-FOPID and KSM-FOPID.

Algorithm	J_{\min}	K_p	K_i	K_d	λ	μ
KSM-FOPID [25]	0.00382	0.950	4.350	1.250	0.660	0.700
RPEO-FOPID [22]	0.00181	3.7923	3.0424	0.5407	1.3496	1.0358
MOEO-FOPID	0.00051	4.9070	4.1614	0.7801	1.0073	1.1391

Figure 8 presents the comparison of frequency deviation, control signal and power deviation of the microgrid with FOPID controllers obtained by MOEO, KSM and RPEO. The corresponding individual powers of different components are shown in Figure 9. It is clear that MOEO-FOPID performed better than KSM-FOPID [25] and RPEO-FOPID [22].



(a) Frequency deviation Δf



(b) Control signal u

Figure 8. Cont.

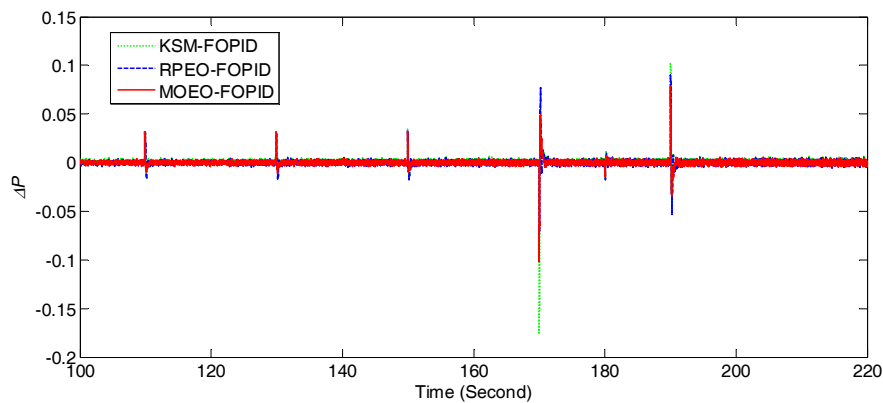
(c) Deficit power deviation ΔP

Figure 8. Comparison of frequency deviation Δf (a), control signal u (b) and deficit power deviation ΔP (c) of the test microgrid with FOPID controllers obtained by the MOEO algorithm and single-objective optimization algorithms including KSM and RPEO.

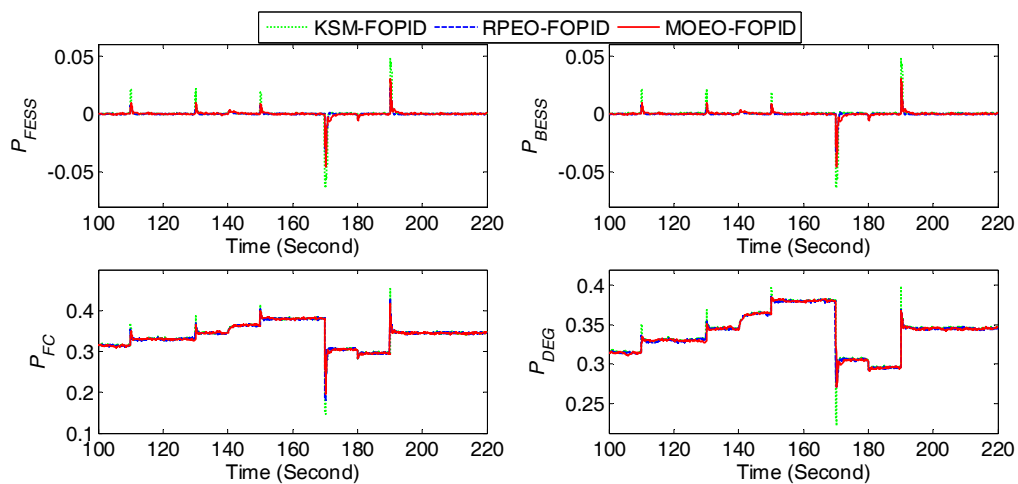


Figure 9. Comparison of individual powers in different components of the test microgrid with FOPID controllers obtained by MOEO and single-objective optimization algorithms including KSM and RPEO.

5.2. Robustness Tests under Perturbed System Parameters

It has been demonstrated that the parametric robustness of FOPID controllers is better than that of PID controllers for the frequency control of an islanded microgrid [25]. In this subsection, the robustness of the best FOPID controllers obtained by MOEO and NSGA-II under perturbed system parameters are compared. Figures 10 and 11 present the comparison of frequency deviation under both increased and decreased system parameters, e.g., D , H , R , T_{FC} , T_g and T_t , respectively. Clearly, the frequency deviations with the FOPID controller optimized by MOEO were still smaller than those by NSGA-II in all the cases. In other words, MOEO-FOPID is superior to NSGA-II in terms of parametric robustness.

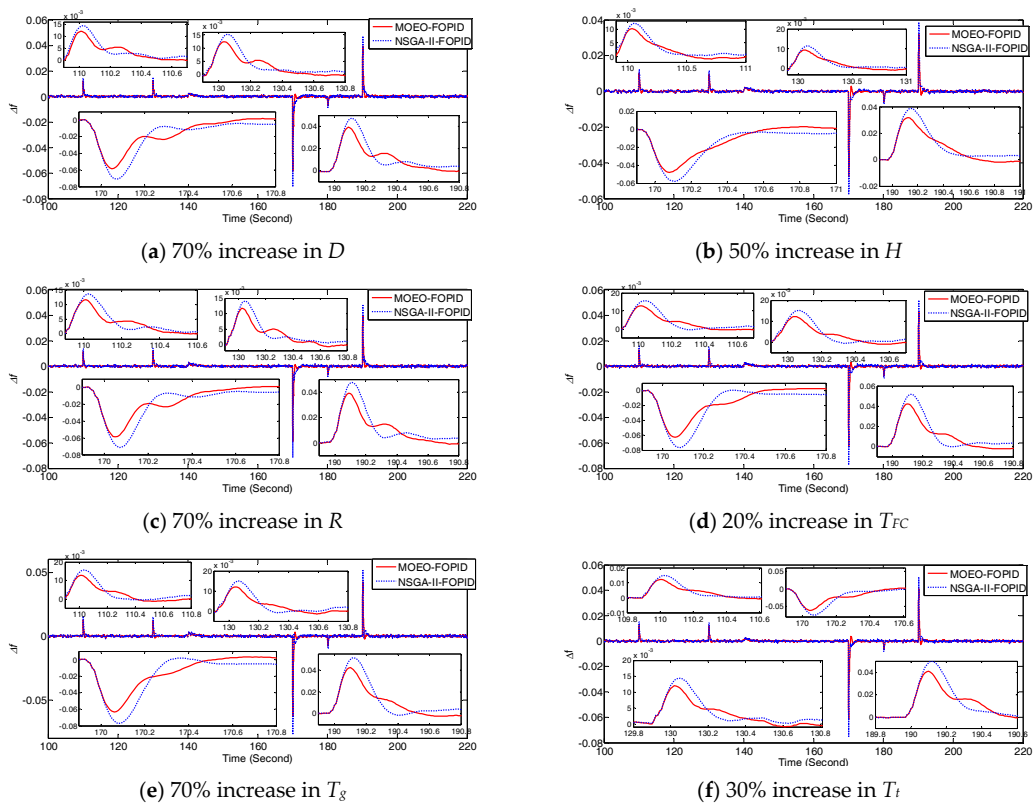


Figure 10. Comparison of the robustness against increased system parameters obtained by MOEO-FOPID and NSGA-II-FOPID.

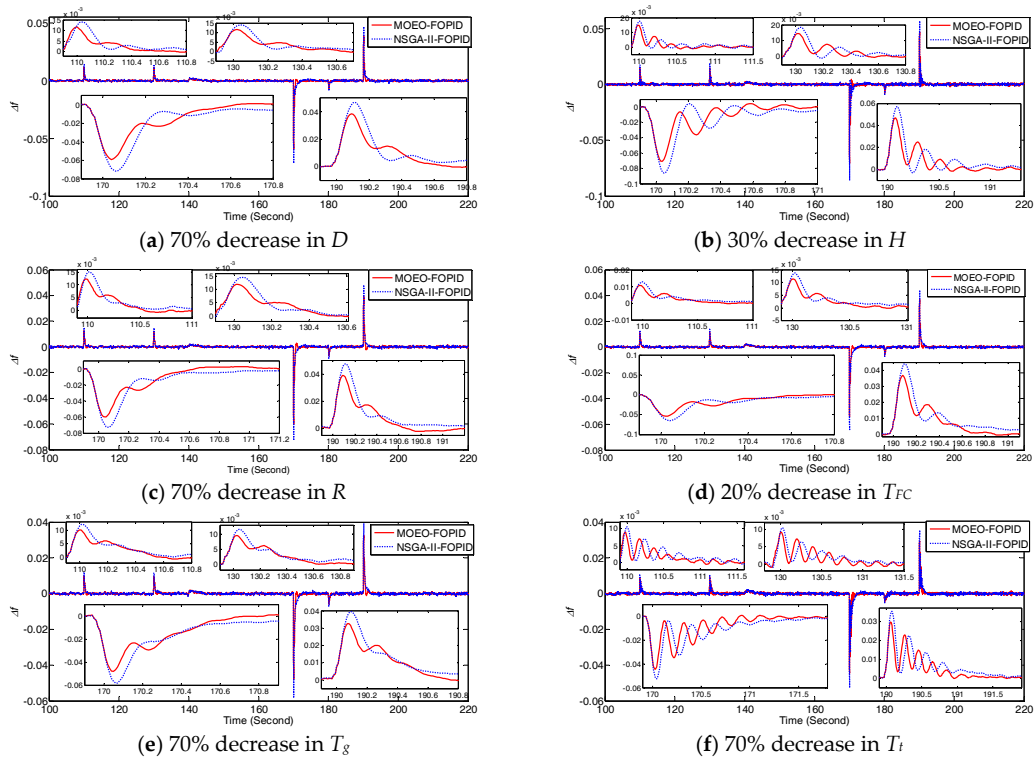


Figure 11. Comparison of the robustness against decreased system parameters obtained by MOEO-FOPID and NSGA-II-FOPID.

6. Conclusions

In this paper, an effective fractional order frequency PID controller design method called MOEO-FOPID was proposed for an islanded microgrid, by using a multi-objective extremal optimization algorithm to improve the efficient operation of distributed generations and energy storage devices. The simulation studies for the case of islanded microgrid showed that the proposed MOEO-FOPID outperforms NSGA-II-based FOPID/PID controllers [20,38], a MOEO-based PID controller, and also other reported single-objective optimization methods, e.g., Kriging-based surrogate modeling and real-coded population-EO-based FOPID controllers [22,25] in terms of smaller frequency deviation, grid power deficit, and control signal. Furthermore, MOEO-FOPID had stronger robustness against perturbed system parameters than NSGA-II-based FOPID controllers. The reasons for the superiority of MOEO-FOPID compared to NSGA-II-FOPID are that MOEO-FOPID has an efficient individual based iterated optimization mechanism with simpler operations and it has more possibility to search the real Pareto-optimal set. Consequently, the proposed MOEO-FOPID can be considered as a competitive multi-objective optimization method for the fractional order frequency control of an islanded microgrid from the perspective- of the complexity of algorithm design and computational efficiency. Of course, the frequency control performance of an islanded microgrid can be further improved by other improved multi-objective evolutionary algorithms and advanced control structures, e.g., robust loop shape controllers and model predictive controllers. Furthermore, the basic idea behind the proposed MOEO-FOPID method can be extended to the optimal control of more complex power systems.

Acknowledgments: The authors gratefully acknowledge the helpful comments and suggestions of editors and anonymous reviewers. This work was partially supported by Zhejiang Provincial Natural Science Foundation of China (Nos.LY16F030011 and LZ16E050002), the National Natural Science Foundation of China (No. 51207112), and Zhejiang Province Science and Technology Planning Project (Nos.2014C31074, 2014C31093, and 2015C31157).

Author Contributions: Huan Wang designed the main algorithm and the software; Guoqiang Zeng proposed the novel idea and the algorithm framework and wrote the manuscript; Yuxing Dai designed the comparative algorithms, e.g., NSGA-II, KSM and PEO; Daqiang Bi performed the simulation for the test microgrid; Jingliao Sun analyzed the simulation results and improved the language; Xiaoqing Xie provided the small-signal model of an islanded microgrid. All authors approved the final manuscript.

Conflicts of Interest: The authors declare no conflict of interest.

References

1. Mahmoud, M.S.; Hussain, S.A.; Abido, M.A. Modeling and control of microgrid: An overview. *J. Frankl. Inst.* **2014**, *351*, 2822–2859. [[CrossRef](#)]
2. Olivares, D.E.; Mehrizi-Sani, A.; Etemadi, A.H.; Canizares, C.A.; Iravani, R.; Kazerani, M.; Hajimiragha, A.H.; Gomis-Bellmunt, O.; Saadefard, M.; Palma-Behnke, R.; et al. Trends in microgrid control. *IEEE Trans. Smart Grid* **2014**, *5*, 1905–1919. [[CrossRef](#)]
3. Lidula, N.W.A.; Rajapakse, A.D. Microgrids research: A review of experimental microgrids and test systems. *Renew. Sustain. Energy Rev.* **2011**, *15*, 186–202. [[CrossRef](#)]
4. Kamel, R.M. New inverter control for balancing standalone micro-grid phase voltages: A review on MG power quality improvement. *Renew. Sustain. Energy Rev.* **2016**, *63*, 520–532. [[CrossRef](#)]
5. Mariam, L.; Basu, M.; Conlon, M.F. Microgrid: Architecture, policy and future trends. *Renew. Sustain. Energy Rev.* **2016**, *64*, 477–489. [[CrossRef](#)]
6. Zhao, Z.; Yang, P.; Guerrero, J.M.; Xu, Z.; Green, T.C. Multiple-time-scales hierarchical frequency stability control strategy of medium-voltage isolated microgrid. *IEEE Trans. Power Electron.* **2016**, *31*, 5974–5991. [[CrossRef](#)]
7. Pandey, S.K.; Mohanty, S.R.; Kishor, N. A literature survey on load-frequency control for conventional and distribution generation power systems. *Renew. Sustain. Energy Rev.* **2013**, *25*, 318–334. [[CrossRef](#)]
8. Lee, D.J.; Wang, L. Small-signal stability analysis of an autonomous hybrid renewable energy power generation/energy storage system part I: Time-domain simulations. *IEEE Trans. Energy Convers.* **2008**, *23*, 311–320. [[CrossRef](#)]

9. Ray, P.K.; Mohanty, S.R.; Kishor, N. Proportional–integral controller based small-signal analysis of hybrid distributed generation systems. *Energy Convers. Manag.* **2011**, *52*, 1943–1954. [[CrossRef](#)]
10. Dahal, S.; Mithulananthan, N.; Saha, T.K. Assessment and enhancement of small signal stability of a renewable-energy-based electricity distribution system. *IEEE Trans. Sustain. Energy* **2012**, *3*, 407–415. [[CrossRef](#)]
11. Bevrani, H.; Habibi, F.; Babahajyani, P.; Watanabe, M.; Mitani, Y. Intelligent frequency control in an AC microgrid: Online PSO-based fuzzy tuning approach. *IEEE Trans. Smart Grid* **2012**, *3*, 1935–1944. [[CrossRef](#)]
12. Divshali, P.H.; Alimardani, A.; Hosseini, S.H.; Abedi, M. Decentralized cooperative control strategy of microsources for stabilizing autonomous vsc-based microgrids. *IEEE Trans. Power Syst.* **2012**, *27*, 1949–1959. [[CrossRef](#)]
13. Das, D.C.; Roy, A.K.; Sinha, N. GA based frequency controller for solar thermal-diesel-wind hybrid energy generation/energy storage system. *Int. J. Electr. Power Energy Syst.* **2012**, *43*, 262–279. [[CrossRef](#)]
14. Singh, V.P.; Mohanty, S.R.; Kishor, N.; Ray, P.K. Robust H-infinity load frequency control in hybrid distributed generation system. *Int. J. Electr. Power Energy Syst.* **2013**, *46*, 294–305. [[CrossRef](#)]
15. Bevrani, H.; Feizi, M.R.; Ataee, S. Robust frequency control in an islanded microgrid: H_{∞} and μ -Synthesis Approaches. *IEEE Trans. Smart Grid* **2016**, *7*, 706–717.
16. Bendato, I.; Bonfiglio, A.; Brignone, M.; Delfino, F.; Pampararo, F.; Procopio, R. A real-time energy management system for the integration of economical aspects and system operator requirements: Definition and validation. *Renew. Energy* **2017**, *102*, 406–416. [[CrossRef](#)]
17. Podlubny, I. Fractional-order systems and $PI^{\lambda}D^{\mu}$ controllers. *IEEE Trans. Autom. Control* **1999**, *44*, 208–213. [[CrossRef](#)]
18. Chen, Y.Q.; Petráš, I.; Xue, D.Y. Fractional order control—A tutorial. In Proceedings of the 2009 American Control Conference, St. Louis, MO, USA, 10–12 June 2009; pp. 1397–1411.
19. Monje, C.A.; Chen, Y.Q.; Vinagre, B.M.; Xue, D.; Feliu-Batlle, V. *Fractional-Order Systems and Controls: Fundamentals and Applications*; Springer Science & Business Media: Berlin, Germany, 2010.
20. Meng, L.; Xue, D. Design of an optimal fractional-order PID controller using multi-objective GA optimization. In Proceedings of the Control and Decision Conference CCDC, Guilin, China, 17–19 June 2009; pp. 3849–3853.
21. Pan, I.; Das, S. Chaotic multi-objective optimization based design of fractional order $PI^{\lambda}D^{\mu}$ controller in AVR system. *Int. J. Electr. Power Energy Syst.* **2012**, *43*, 393–407. [[CrossRef](#)]
22. Zeng, G.Q.; Liu, H.Y.; Wu, D.; Li, L.M.; Wu, L.; Dai, Y.X.; Lu, K.D. A real-coded extremal optimization method with multi-non-uniform mutation for the design of fractional order PID controllers. *Inf. Technol. Control* **2016**, *45*, 358–375. [[CrossRef](#)]
23. Ahmed, B.S.; Sahib, M.A.; Gambardella, L.M.; Afzal, W.; Zamli, K.Z. Optimum design of $PI^{\lambda}D^{\mu}$ controller for an automatic voltage regulator system using combinatorial test design. *PLoS ONE* **2016**, *11*, e0166150. [[CrossRef](#)] [[PubMed](#)]
24. Wu, D.; Wang, H.; Zeng, G.Q.; Lu, K.D. Design of fractional-order PID controllers for fractional-order systems: A binary-coded individual-based extremal optimization method. *ICIC Express Lett.* **2016**, *10*, 2191–2196.
25. Pan, I.; Das, S. Kriging based surrogate modeling for fractional order control of microgrids. *IEEE Trans. Smart Grid* **2015**, *6*, 36–44. [[CrossRef](#)]
26. Pan, I.; Das, S. Fractional order fuzzy control of hybrid power system with renewable generation using chaotic PSO. *ISA Trans.* **2016**, *62*, 19–29. [[CrossRef](#)] [[PubMed](#)]
27. Pan, I.; Das, S. Fractional-order load-frequency control of interconnected power systems using chaotic multi-objective optimization. *Appl. Soft Comput.* **2015**, *29*, 328–344. [[CrossRef](#)]
28. Boettcher, S.; Percus, A. Nature’s way of optimizing. *Artif. Intell.* **2000**, *119*, 275–286. [[CrossRef](#)]
29. Boettcher, S.; Percus, A.G. Optimization with extremal dynamics. *Phys. Rev. Lett.* **2001**, *86*, 5211. [[CrossRef](#)] [[PubMed](#)]
30. Bak, P.; Sneppen, K. Punctuated equilibrium and criticality in a simple model of evolution. *Phys. Rev. Lett.* **1993**, *71*, 4083. [[CrossRef](#)] [[PubMed](#)]
31. Lu, Y.Z.; Chen, Y.W.; Chen, M.R.; Chen, P.; Zeng, G.Q. *Extremal Optimization: Fundamentals, Algorithms, and Applications*; CRC Press & Chemical Industry Press: Boca Raton, FL, USA, 2016.
32. Dai, Y.X.; Wang, H.; Zeng, G.Q. Double closed-loop PI control of three-phase inverters by binary-coded extremal optimization. *IEEE Access* **2016**, *4*, 7621–7632. [[CrossRef](#)]

33. Chen, M.R.; Lu, Y.Z. A novel elitist multiobjective optimization algorithm: Multiobjective extremal optimization. *Eur. J. Oper. Res.* **2008**, *188*, 637–651. [[CrossRef](#)]
34. Chen, M.R.; Lu, Y.Z.; Yang, G. Multiobjective optimization using population-based extremal optimization. *Neural Comput. Appl.* **2008**, *17*, 101–109. [[CrossRef](#)]
35. Randall, M.; Lewis, A. Population extremal optimization for discrete multi-objective optimization problems. *Inf. Sci.* **2016**, *367*, 390–402. [[CrossRef](#)]
36. Zeng, G.Q.; Chen, J.; Li, L.M.; Chen, M.R.; Wu, L.; Dai, Y.X.; Zheng, C.W. An improved multi-objective population-based extremal optimization algorithm with polynomial mutation. *Inf. Sci.* **2016**, *330*, 49–73. [[CrossRef](#)]
37. Zeng, G.Q.; Chen, J.; Dai, Y.X.; Li, L.M.; Zheng, C.W.; Chen, M.R. Design of fractional order PID controller for automatic regulator voltage system based on multi-objective extremal optimization. *Neurocomputing* **2015**, *160*, 173–184. [[CrossRef](#)]
38. Deb, K.; Pratap, A.; Agarwal, S.; Meyarivan, T.A.M.T. A fast and elitist multiobjective genetic algorithm: NSGA-II. *IEEE Trans. Evol. Comput.* **2002**, *6*, 182–197. [[CrossRef](#)]
39. Collette, Y.; Siarry, P. *Multiobjective Optimization: Principles and Case Studies*; Springer Science & Business Media: Berlin, Germany, 2013.
40. Li, L.M.; Lu, K.D.; Zeng, G.Q.; Wu, L.; Chen, M.R. A novel real-coded population-based extremal optimization algorithm with polynomial mutation: A non-parametric statistical study on continuous optimization problems. *Neurocomputing* **2016**, *174*, 577–587. [[CrossRef](#)]



© 2017 by the authors. Licensee MDPI, Basel, Switzerland. This article is an open access article distributed under the terms and conditions of the Creative Commons Attribution (CC BY) license (<http://creativecommons.org/licenses/by/4.0/>).